EASR

Engineering and Applied Science Research

https://www.tci-thaijo.org/index.php/easr/index

Published by the Faculty of Engineering, Khon Kaen University, Thailand

Experimental and numerical investigation of 2-dimensional heat pipe wall temperature profile

Kittinan Wansasueb[1)], Pitak Promthaisong[2)], Bopit Bubphachot[2)], Adisak Pattiya[3)], Teerapat Chompookham[2)], Sampan Rittidech[2)] and Narin Siriwan*[2)]

[1)]Electronics for Agriculture Research Unit, Faculty of Engineering, Mahasarakham University, Maha Sarakham, Thailand
[2)]Heat Pipe and Thermal Equipment Research Unit, Faculty of Engineering, Mahasarakham University, Maha Sarakham, Thailand
[3)]Bio-Energy and Renewable Resources Research Unit, Faculty of Engineering, Mahasarakham University, Maha Sarakham, Thailand

Received 15 December 2022
Revised 31 July 2023
Accepted 29 August 2023

Abstract

This study focuses on the numerical validation of a two-dimensional model of a heat pipe's temperature profile under transient conditions. The model was constructed from copper, and the finite difference method was employed as the numerical solver. The study recorded the temperature distribution at the pipe wall in the evaporator, adiabatic and condenser sections, with a focus on the initial temperatures of the evaporator section. The temperatures at the pipe wall were compared with the numerical computation solutions. The results showed an agreement between the experimental and numerical temperature profiles with percentage error between 4.463 and 5.900 %.

Keywords: Heat pipe, Two-dimensional model, Temperature profiles, Finite difference method

Nomenclature

C_p	specific heat (J/kg*k)
L	length (m)
R	radius (m)
T	temperature (°C)
k	thermal conductivity (W/m*k)
r	length along r direction (m)
t	time (s)
y	length along y direction (m)

Greek letter

ρ	density (kg/m^3)

Sub-script

a	adiabatic
c	condenser
e	evaporator
i	inlet
w	wall

1. Introduction

Heat pipes are passive heat transfer devices that can efficiently recover waste heat from a system without requiring external energy input [1]. Heat pipes have found applications in various fields such as electronic and electrical packaging, production tools, engines, solar energy systems and heat exchangers [2-4], and related industries [5-8]. Heat pipes possess two working states, which are transient or transition [9-14], and steady state [9-17]. As the heat pipes transition from one state to another, their temperature increases [18-20]. Once they reach a steady state, where the final temperature remains constant, maximum heat transfer can be achieved. To design and construct a heat pipe with maximum heat transfer, it is crucial to accurately predict the time required for the heat pipe to reach a steady state during the heating up process [21, 22]. The prediction can be performed via mathematical models [2, 23-29], which are accurate and reliable. These models are typically developed with computer software [2, 16, 17, 29]. For instance, Huang and Chen [11] presented a numerical model for heat pipes using the lattice Boltzmann method. Their results demonstrated that the numerical outputs were in good agreement with the literature model, indicating their model's validity. Another noteworthy study was conducted by Siriwan et al. in 2017, who presented a numerical model and experimental validation for a helical oscillating heat pipe (HOHP) [16, 17]. Additionally, Zhang et al. investigated the use of a CO_2 loop thermosyphon for free cooling of data centers using both experimental and numerical approaches [28]. To achieve high-performance thermal equipment design, a continuous improvement of numerical methods for heat transfer in microfluidics has been pursued [30-34]. Example applications include natural convection [35, 36] and cavity flow with heat transfer problems [37]. Additionally, the finite element method is a popular approach [38-40], although it can be computationally intensive.

To design heat pipes, various shapes have been considered, including a single loop pulsating heat pipe for which thermal performance was investigated by Patel and Kumar [41]. The thermal characteristics of a flat plate pulsating heat pipe were presented by Li and Li [42], a loop heat pipe with rectangular evaporator was validated by Yang et al. [43], and additionally, the thermal performance of a flat heat pipe (HTFHP) with applied high temperature conditions was investigated by Xu et al. [44]. To enhance the

*Corresponding author.
Email address: narin.s@msu.ac.th
doi: 10.14456/easr.2023.48

design methodology of heat pipes, the incorporation of an effective analytical tool is crucial. While both numerical and experimental approaches offer promising methods, they need to be validated for reliability and accuracy before implementation.

The aim of this work is to validate the temperature profile in the two-dimensional transient model, in order to establish a baseline for the heat pipe design procedure. The concept of the temperature distribution was proposed by Faghri [1]. Experiments were conducted using a copper mesh wick heat pipe and temperature distribution was illustrated as a function of time. The validation results of the model were investigated while a finite difference method was used to compute a numerical simulation. The numerical and experimental results of all three zones of the heat pipe and their temperature profiles were compared and discussed. The times consumed to achieve a steady-state between numerical and experimental data were compared.

2. Conceptual framework

2.1 Two-Dimensional model heat pipe governing equation

The proposed model was formulated based on thermophysical properties; the wall properties were constant throughout the operation [1].

The heat pipe model of this study is illustrated in Figure 1. The model was constructed with three sections, comprising an evaporator section, an adiabatic section and a condenser section. The governing equation of the two-dimensional heat conduction is given by equation (1) [1].

$$\rho_w \, C_{p,w} \frac{\partial T}{\partial t} = k_w \frac{1}{r} \frac{\partial}{\partial r}\left(r \frac{\partial T}{\partial r}\right) + k_w \left(\frac{\partial^2 T}{\partial y^2}\right) \tag{1}$$

where ρ_w is the density of the pipe wall, $C_{p,w}$ is the specific heat of the pipe wall, and k_w is the thermal conductivity of the pipe wall.

In the method used for the analysis, the temperature at the wall was separated into three time zones. The initial state ($t = 0$) was that in which the temperature was applied at the evaporator outer skin. In the second zone the temperature was rising at the pipe wall. The system eventually achieved a steady state. The temperature input was stored in the pipe wall, so the wall temperature increased with time. An amount of heat is transferred to the condenser section with a gradual and increasing rate, such that the condenser temperature equals that of temperature input; this is referred to as the steady state. The initial temperature of the evaporator wall is given by equation (2).

$$t = 0, \quad T = T_i \tag{2}$$

where T_i is the uniform initial condition temperature.

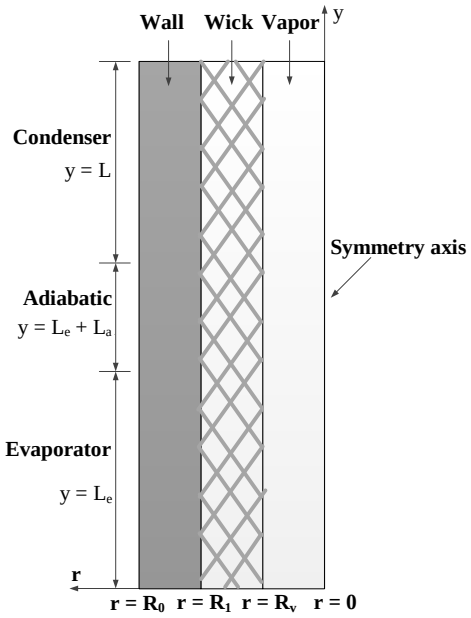

Figure 1 Coordinate system

For the experimental setup, the temperature of the evaporator section was kept constant while the adiabatic section was insulated, and heat was removed at the condenser section by cooling water. All of the three boundary zone conditions can be written as equation (3).

$$\left\{ \begin{array}{ll} T_e = 70, 80, 90°C & 0 \le y < L_e \\ \frac{\partial T}{\partial r} = 0 & L_e \le y < L_e + L_a \\ T_c = 20°C & L_e + L_a \le y < L \end{array} \right\} \tag{3}$$

The flow rate at the condenser is assumed to be laminar. At the wall-wick, the heat transfer is neglected. Thus,

$\frac{\partial T}{\partial r} = 0$ at $r = R_i$ for all y
$\frac{\partial T}{\partial y} = 0$ at $y = 0$ and $y = L$

2.2 The finite difference technique

The finite difference technique was used to solve for the boundary conditions and the governing equations [1]. The approximation scheme was applied with a five-point second-order central difference approximation [16, 17]. Following this method, the four inner points were used to compute the boundary grid. The Forward Time Center Space method (FTCS) was applied to compute the governing equations. These equations are presented as parabolic equations in which the coefficients are constant. Then, the FTCS makes the governing equation into non-linear equations. According to this scheme, at time *t* in every node, the temperature is established. At time $t + \Delta t$ for each node, the temperature is calculated using the values of neighboring nodes at time *t*. The marching procedure was continued until reaching a steady-state temperature. The time step was estimated using consistency criteria. The solution procedure was carefully designed. At the initial state, the time required for the temperature to obtain steady state was computed by capturing the development of the temperature distribution at the evaporator wall. After the wall temperature started rising from the initial value, it can be said that the temperature had reached the transient temperature.

2.3 Numerical setup and grid independence check

The time step was computed following the model grid size, so when the number of grids increased, it would reduce the time step. In this case, the time step was set as 10^{-5} sec. The grid independence test was computed and validated. The results were the percentage change at the steady state from device sections, including the evaporator, adiabatic and condenser sections. The results of the grid independence test included 5 × 12 and 10 × 24 grid points (radial and axial, respectively). The outer wall temperature at the evaporator section was set as 60°C and was validated as shown in Table 1. In both models, the error at the steady-state was less than 1%. The 10 × 24 grid size consumed more computation time than the 5 × 12 grid size. Therefore, the 5 × 12 grid size was used in this study. In this model, the dimensions were 2×10^{-4} meters in the radial axis for the pipe wall while in the axial direction the dimension was 2×10^{-3} meters.

Table 1 Grid independence check

Heat pipe section	5x12	10x24	Change (%)
Evaporator	77.4937	77.4498	0.057
Adiabatic	49.2191	49.2070	0.025
Condenser	20.0888	20.0901	0.006

2.4 Experimental setup

The heat pipe in this study was constructed of copper and sealed at both the ends with copper caps. The geometry of the pipe is 270 mm long, 12.7 millimeter outer-diameter and a 1.4-millimeter wall thickness. The working fluid was water. The material properties of the heat pipe are given in Table 2 and the set-up of the laboratory experiment is shown in Figure 2. The evaporator and condenser sections were hot and cool respectively and temperatures were maintained by water cooling in acrylic boxes [45] of 150 × 150 × 150 mm (width × length × height). Both boxes were covered with Aeroflex insulation. The adiabatic section was also insulated with Aeroflex. The water flow in the hot and the cool water jackets were measured by a flow meter, while the cool water jacket was insulated. Both the hot and cool water inputs must have a constant initial temperature. They are controlled using a heater with temperature control at the hot section and a cool bath at the cool section (details in Figure 2). Seven thermocouples (type K) were attached to the outside wall of the heat pipe at all sections, and temperature data were collected using a data logger. All thermocouples were calibrated against any variation in the room temperature.

Table 2 The geometry specifications of heat pipe and material properties.

Model geometry	Copper
Pipe outer diameter (D_o)	12.7×10^{-3}m
Pipe inner diameter (D_i)	11.3×10^{-3}m
Pipe length (L)	0.27m
Evaporator section length (L_e)	0.11m
Adiabatic section length (L_a)	0.05m
Condenser section length (L_c)	0.11m
Thermal conductivity k_w	401 w/m K
Density ρ_w	8933 kg/m^3
Specific heat capacity $C_{p,w}$	385 J/kg K

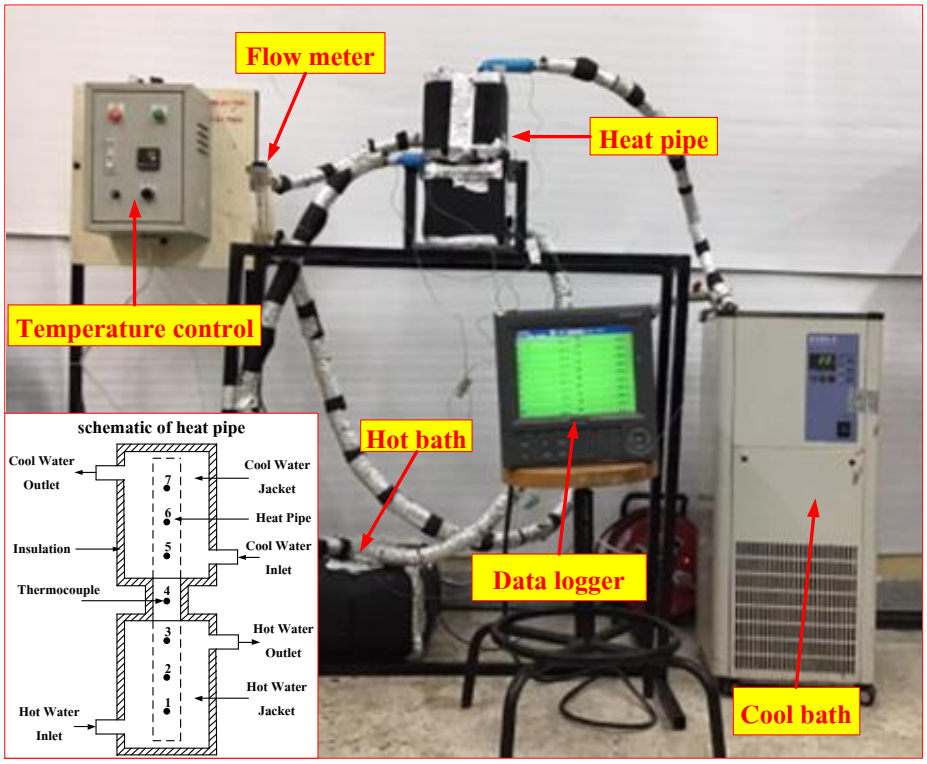

Figure 2 The experimental set-up

Based on the experimental device mentioned above, this study was limited to assessing the performance of the laboratory device. The testing process begins at the initial state (*t=0*); the heater was turned on to input the temperature using water in the hot water jacket and the water then flowed to the evaporator section. At the same time, the cooling water flowed to the condenser section. The outer wall temperatures and the water inlet and outlet temperatures were recorded at intervals of 2 sec. The cool water flow rate was carefully measured during each time interval. The heat recovery from the condenser was measured by means of the water inlet and outlet temperatures until it reached a steady state. The input of the outer wall temperature of the evaporator section were 70, 80 and 90°C and a temperature input at the outer wall of the condenser section of 20 °C was used for the experiments. The percentage error between the numerical and experimental temperature profiles is computed following equation (4)

$$\%error = abs(\frac{T_E - T_N}{T_E}) \times 100 \quad (4)$$

where

T_E is the temperature profile resulting from the experiment and

T_N is the temperature profile resulting from numerical computation.

The temperature profiles from both numerical simulations and experimental data are presented. In the steady state, the percentage errors from both methods are discussed in the next section.

3. Results and discussion

In this section, both numerical and experimental temperature profile results of the heat pipe are compared. The three case studies involved temperatures of 70, 80 and 90 °C of the evaporator section.

3.1 Evaporator section temperature 70°C

The comparative temperature profiles of numerical and experimental results of the 70°C evaporator heat pipe are shown in Figure 3. All of the evaporator, adiabatic and condenser temperature profiles are presented. As seen in the figure, the profile comes to steady state at 1322 and 1400 seconds for experimental and numerical results respectively. The details are presented in Appendix Table A1, with the steady state point indicated in bold. For the experimental result, the evaporator section experienced a linearly increasing temperature and then was constant at a steady state temperature of 65.6 °C, while the numerical result given an absolute horizontal parabola profile and was constant at a steady state temperature of 70 °C following the boundary condition setup. The adiabatic section profiles of both simulation and experimental results were similar to the evaporator section, while the steady state temperatures were 45 and 42.4 °C respectively. For the condenser section, both model and experiment had the same profile at around 20 °C at the final state. At the final state, the percentage error at the steady state temperature of all three sections was 6.7%, 6.1% and 0.5% for evaporator, adiabatic and condenser section respectively.

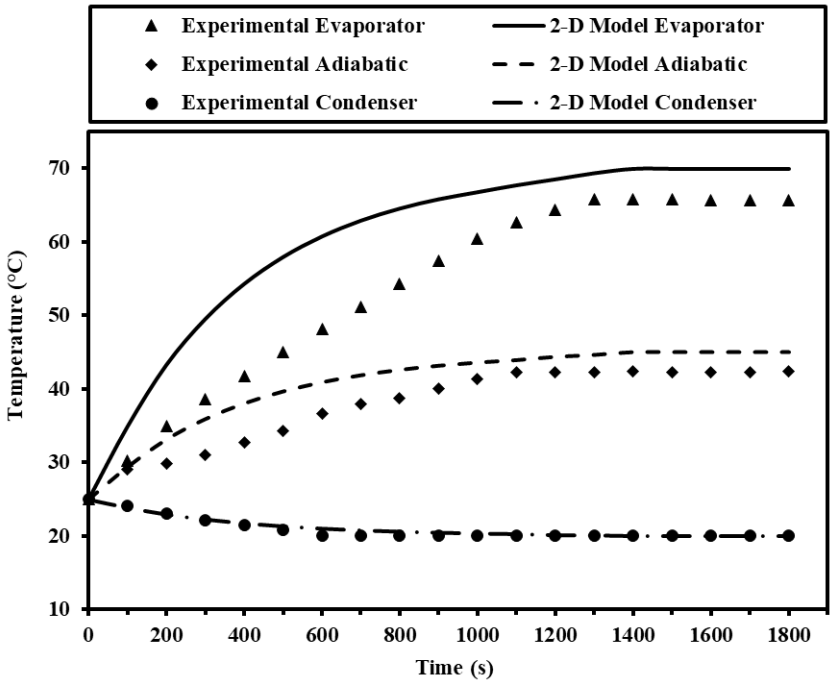

Figure 3 Temperature profiles of heat pipe wall comparison for T_e = 70°C.

3.2 Evaporator section temperature of 80°C

The second case study compared temperature profiles between numerical and experimental results of the 80°C evaporator heat pipe (shown in Figure 4). As with the 70°C evaporator heat pipe results described above, all of the evaporator, adiabatic and condenser temperature profiles are presented. It is seen from the figure that the temperature profile came to a steady state in 1718 and 1800 seconds for experiment and numerical results respectively. The details are presented in Appendix Table A2 with the steady state point indicated in bold. Numerical and experimental results had related temperature profiles. In contrast at the steady state, the simulation result achieved a final temperature value of 80 °C, while the experimental result gave a value of 74.7 °C. As with the evaporator temperature profile described above, the temperature profile of the adiabatic section in both simulation and experimental results behaved similarly, while the steady state temperatures were 50 and 47.0 °C respectively. For the condenser section, both model and experiment had the same profile at around 20 °C at the final state. At the final state, the percentage errors at steady state temperature of all three sections were 7.2%, 6.4% and 1.0% for evaporator, adiabatic and condenser section respectively.

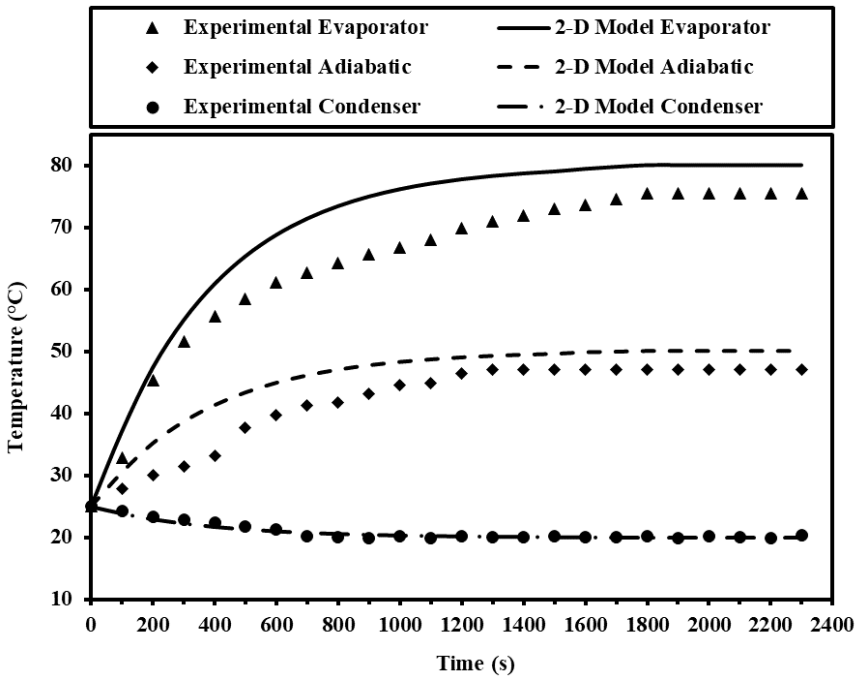

Figure 4 Temperature profile comparisons of heat pipe wall for T_e = 80°C

3.3 Evaporator section temperature of 90°C

The last case study presents the comparative temperature profile results of the 90°C evaporator heat pipe (shown in Figure 5). The increasing temperature profile behavior was similar to that of the 80°C profile. However, the temperature profile came to a steady state at 2106 and 2200 seconds for experiment and numerical results respectively. The details are presented in Appendix Table A3 with the steady state point indicated in bold. At the steady state, the simulation result was similar to the experimental result, with a final temperature value around 90 °C. The temperature profiles of the adiabatic section, in both simulation and experimental results, were similar to the steady state temperatures of 55 and 52.9 °C respectively. For the condenser section, both model and experimental results had the same profile at around 20 °C at the final state. At the final state, the percentage error at steady state temperature of all three sections was 1.6%, 4.0% and 0.5% for evaporator, adiabatic and condenser section respectively.

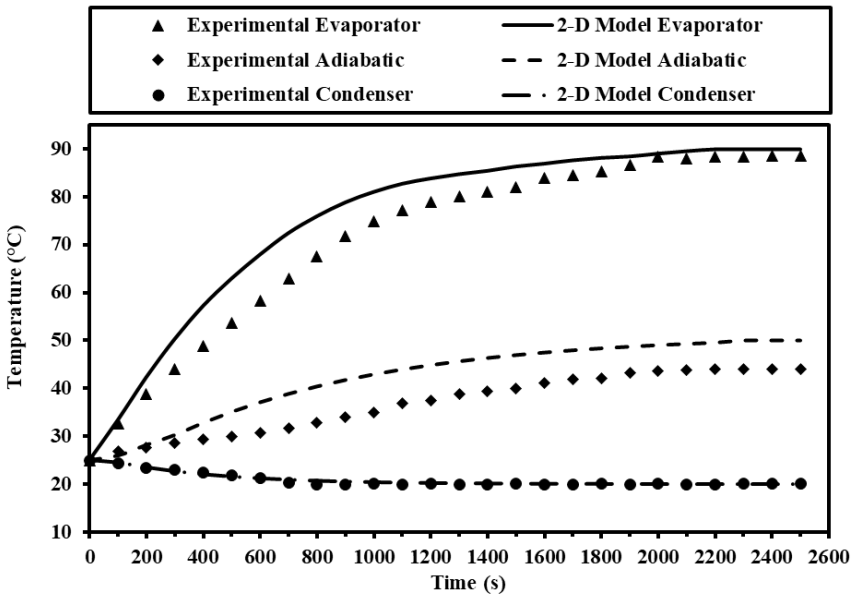

Figure 5 Temperature profiles of heat pipe wall for T_e = 90°C

Finally, the total time consumption is presented in Table 3 for all case studies. The results from the experimental and the two-dimensional model are summarized and compared. All the experimental cases show that the time required to arrive at the steady state was less than the numerical result, with percentage errors of 5.9%, 4.773% and 4.463% for the cases of evaporator temperature of 70, 80 and 90 °C respectively. At steady state, in all case studies, it was observed that in the evaporator section, the final temperature for the experimental results did not reach the final temperature indicated by the numerical results. This discrepancy can be attributed to the intrinsic limitations of the laboratory setup, which could not control external factors such as surrounding temperature, humidity and atmospheric pressure. These external factors can influence the working fluid in the test section, where water is used as an intermediary to transfer heat from the source to the heat pipe wall (evaporator section). It is possible that heat was lost due to the latent heat of evaporation of the water. Consequently, the temperature profile trend in the experimental results consistently exhibited lower values than the numerical results for all cases at 70, 80 and 90 °C.

Table 3 Transient response of the heat pipe

	Total time consumed (second)		
Evaporator Temperature (°C)	**Experimental**	**Numerical**	**Error (%)**
70	1322	1400	5.900
80	1718	1800	4.773
90	2106	2200	4.463

The second investigation consists of a comparison with previous work. Traditional research on the temperature profiles of a spiral heat pipe has been presented by Siriwan et al. [17]. The temperature profiles are presented for the numerical results of the 80°C evaporator case (Figure 6). Following Figure 6, it is seen that the temperature profile of the present work had a sharper increasing slope than the spiral case in the rising region, and was then constant at final temperatures of 80 and 73.5 for the present work and the spiral case respectively. The results conform with the loop heat pipe experimental results presented by Hashimoto et al. [46], who presented a comparison between numerical and experimental results for the loop heat pipe in an electric vehicle battery. The results confirm that the numerical behavior agrees with the experimental behavior, with a difference in temperature of approximately 0.06 – 0.09 °C/min. Also, Abela et al. [47] presented an experimental analysis and transient numerical simulation of a large diameter pulsating heat pipe in microgravity conditions. The result showed that for simulations run for different power levels, the results were comparable with the experimental data, showing that the model can predict the device behavior. Both related works [46, 47] used operating temperatures of about 20 to 100 °C, confirming that a numerical study is more popular at the present time, and the validation case studies are reliable and acceptable.

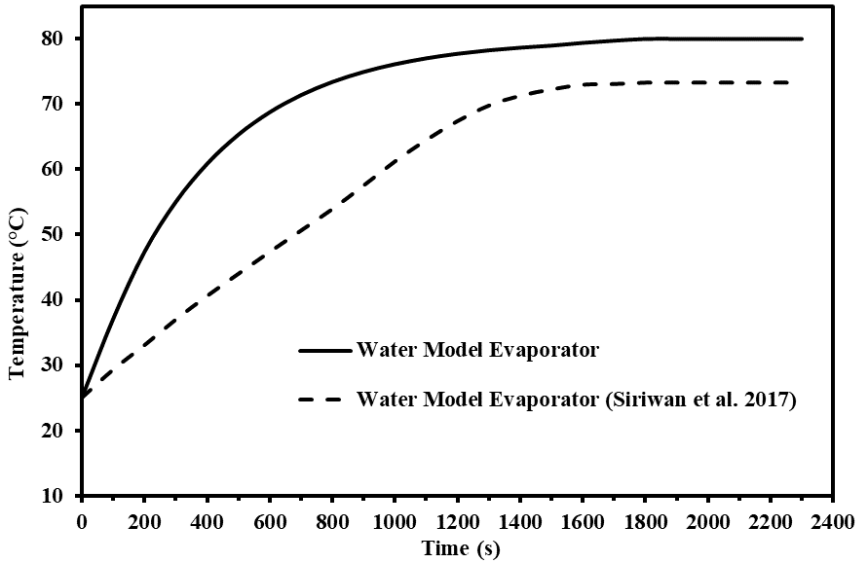

Figure 6 A comparison of temperature profiles in the adiabatic section of this study and Siriwan et al. [17]

4. Conclusions

The temperature profile of a heat pipe was investigated, using both numerical and experimental results, which were compared and discussed. Three case studies using 70, 80 and 90°C evaporator temperatures were analyzed. Numerical solutions were compared with experimental results.

- The experimental results required less time to reach steady state than did the numerical results.
- The precision of the numerical outcomes was evaluated in three different sections of the heat pipe, the evaporator, adiabatic and condenser sections. The results reveal that the margin of error for the evaporator section was within the range of 1.6% to 7.2%, while for the adiabatic section, the error was between 4.0% and 6.4%. For all input temperatures studied (70, 80 and 90°), the condenser section error was less than 1.0%. In addition, the numerical findings indicated higher values compared to all computation results as presented in Figures 3 to 5.

The second investigation compared existing research (Siriwan et al. [17]) and found that the straight pipe was more effective than the spiral pipe at the region of the time domain as shown in Figure 6.

This research serves as the foundation for improving heat pipe technology. Further studies will focus on exploring various shapes and sizes to enhance heat pipe performance, including high-temperature heat pipes which are often used for cooling reactor devices [48-50]. The methods used to improve the performance of high-temperature heat pipes will be similar to those of general heat pipes.

5. Acknowledgements

This research project was financially supported by Faculty of Engineering Mahasarakham University.

6. References

[1] Faghri A. Heat pipe science and technology. 2nd ed. Global Digital Press; 2016.
[2] Musediq AS, Yahaya A, Olanrewaju BO, Babatunde OA, Solomon OG. Computational analysis of water-based copper oxide nanofluid properties and performance in a double-pipe small-scale heat exchanger. Eng Appl Sci Res. 2021;48(2):161-70.
[3] Prasopsuk C, Hoonpong P, Skullong S, Promvonge P. Experimental investigation of thermal performance enhancement in tubular heat exchanger fitted with rectangular-winglet-tape vortex generator. KKU Eng J. 2016;43(S2):279-82.
[4] Srimuang W, Khantikomol P, Krittacom B. An experimental investigation of effectiveness of a closed-end flat heat pipe heat exchanger (CEFHPHE). KKU Eng J. 2013;40(1):21-7.
[5] Xia G, Zhuang D, Ding G, Lu J. A quasi-three-dimensional distributed parameter model of micro-channel separated heat pipe applied for cooling telecommunication cabinets. Appl Energy. 2020;276:115544.
[6] Mozafarie SS, Javaherdeh K, Ghanbari O. Numerical simulation of nanofluid turbulent flow in a double-pipe heat exchanger equipped with circular fins. J Therm Anal Calorim. 2021;143:4299-311.
[7] Gawecka KA, Taborda DMG, Potts DM, Sailer E, Cui W, Zdravković L. Finite-element modeling of heat transfer in ground source energy systems with heat exchanger pipes. Int J Geomech. 2020;20(5):1-14.
[8] Xia G, Zhuang D, Ding G, Lu J, Han W, Qi H. A distributed parameter model for multi-row separated heat pipe with micro-channel heat exchangers. Appl Therm Eng. 2021;182:116113.
[9] Altun AH, Bilir S, Ates A. Transient conjugated heat transfer in thermally developing laminar flow in thick-walled pipes and mini-pipes with time periodically varying wall temperature boundary condition. Int J Heat Mass Transf. 2016;92:643-57.
[10] Enke G, Júnior JB, Vlassov V. Transient response of an axially-grooved aluminum-ammonia heat pipe with the presence of non-condensable gas. Appl Therm Eng. 2021;183:116135.
[11] Huang Y, Chen Q. A numerical model for transient simulation of porous wicked heat pipes by lattice Boltzmann method. Int J Heat Mass Transf. 2017;105:270-8.
[12] Joung W, Kim YG, Lee J. Transient characteristics of a loop heat pipe-based hydraulic temperature control technique. Int J Heat Mass Transf. 2016;103:125-32.

[13] Wang G, Liu M, Zhang D, Qiu S, Su GH, Tian W. Experimental study on transient performance of heat pipe-cooled passive residual heat removal system of a molten salt reactor. Prog Nucl Energy. 2020;118:103113.
[14] Xie Y, Zhou Y, Wen D, Wu H, Haritos G, Zhang H. Experimental investigation on transient characteristics of a dual compensation chamber loop heat pipe subjected to acceleration forces. Appl Therm Eng. 2018;130:169-84.
[15] Ismail NR, Soeparman S, Widhiyanuriyawan D, Wijayanti W. Temperature distribution and evaporation rate in porous media. J Southwest Jiaotong Univ. 2020;55(3):1-12.
[16] Siriwan N, Chompookham T, Ding Y, Rittidech S. Mathematical model to predict heat transfer in transient condition of helical oscillating heat pipe. Songklanakarin J Sci Technol. 2017;39(6):765-72.
[17] Siriwan N, Chompookham T, Ding Y, Rittidech S. Heat transfer predictions for helical oscillating heat pipe heat exchanger: transient condition. J Mech Sci Technol. 2017;31:3553-62.
[18] Ma T, Wang X, Zhu T, Li Y. Operation characteristics of a high temperature special shaped heat pipe used in solar thermochemical reactors. Heat Transf Eng. 2019;40(3-4):238-46.
[19] Orr B, Singh R, Akbarzadeh A, Mochizuki M. Operating characteristics of naphthalene heat pipes. Front Heat Mass Transf. 2019;13:1-7.
[20] Auntaisong P, Thinvongpituk C, Sopakayang R, Poonaya S. The study of temperature distribution in steel rods welded by friction welding using computer. KKU Eng J. 2015;42(2):173-83. (In Thai)
[21] Ahmad F, Nazeer M, Saeed M, Saleem A, Ali W. Heat and mass transfer of temperature-dependent viscosity models in a pipe: effects of thermal radiation and heat generation. Zeitschrift für Naturforschung A. 2020;75(3):225-39.
[22] Chen G, Tang Y, Wan Z, Zhong G, Tang H, Zeng G. Heat transfer characteristic of an ultra-thin flat plate heat pipe with surface-functional wicks for cooling electronics. Int Commun Heat Mass Transf. 2019;100:12-9.
[23] Matao P, Reddy BP, Sunzu J. Hall and rotation effects on radiating and reacting MHD flow past an accelerated permeable plate with soret and dufour effects. Trends Sci. 2022;19(5):2879.
[24] Sinha S, Yadav RS. MHD mixed convective slip flow along an inclined porous plate in presence of viscous dissipation and thermal radiation. Trends Sci. 2022;19(4):2685.
[25] Kolliyil JJ, Yarramsetty N, Balaji C. Numerical modeling of a wicked heat pipe using lumped parameter network incorporating the marangoni effect. Heat Transf Eng. 2020;42(9):787-801.
[26] Koito A. Numerical analyses on vapor pressure drop in a centered-wick ultra-thin heat pipe. Front Heat Mass Transf. 2019;13:1-6.
[27] Cui Y, Yu H, Wang H, Wang Z, Yan X. The numerical modeling of the vapor bubble growth on the silicon substrate inside the flat plate heat pipe. Int J Heat Mass Transf. 2020;147:118945.
[28] Zhang H, Shi Z, Liu K, Shao S, Jin T, Tian C. Experimental and numerical investigation on a CO_2 loop thermosyphon for free cooling of data centers. Appl Therm Eng. 2017;111:1083-90.
[29] Siriwan N, Bubphachot B, Eiamsa-ard S, Wongcharee K, Chompookham T, Promthaisong P. 3D Simulation on turbulent flow and heat transfer behaviors in a five-start corrugated tube: effect of depth ratio and tube modification. Eng Appl Sci Res. 2021;48(6):694-703.
[30] Ali N, Nazeer M, Javed T, Abbas F. A numerical study of micropolar flow inside a lid-driven triangular enclosure. Meccanica. 2018;53:3279-3299.
[31] Nazeer M, Ali N, Javed T. Numerical simulation of MHD flow of micropolar fluid inside a porous inclined cavity with uniform and non-uniform heated bottom wall. Can J Phys. 2018;96(6):1-37.
[32] Nazeer M, Ali N, Javed T, Nazir MW. Numerical analysis of the full MHD model with the Galerkin finite-element method. Eur Phys J Plus. 2019;134:204.
[33] Nazeer M, Ali N, Javed T. Numerical simulations of MHD forced convection flow of micropolar fluid inside a right-angled triangular cavity saturated with porous medium: effects of vertical moving wall. Can J Phys. 2019;97(1):1-13.
[34] Nazeer M, Ali N, Javed T. Effects of moving wall on the flow of micropolar fluid inside a right-angle triangular cavity. Int J Numer Methods Heat Fluid Flow. 2018;28(10):2404-22.
[35] Nazeer M, Ali N, Javed T, Asghar Z. Natural convection through spherical particles of a micropolar fluid enclosed in a trapezoidal porous container. Eur Phys J Plus. 2018;133:423.
[36] Nazeer M, Ali N, Javed T. Natural convection flow of micropolar fluid inside a porous square conduit: effects of magnetic field, heat generation/absorption, and thermal radiation. J Porous Media. 2018;21(10):953-75.
[37] Ali N, Nazeer M, Javed T, Siddiqui MA. Buoyancy-driven cavity flow of a micropolar fluid with variably heated bottom wall. Heat Transf Res. 2018;49(5):457-81.
[38] Nazeer M, Ali N, Javed T, Razzaq M. Finite element simulations for energy transfer in a lid-driven porous square container filled with micropolar fluid: impact of thermal boundary conditions and Peclet number. Int J Hydrog Energy. 2019;44(14):7656-66.
[39] Ali N, Nazeer M, Javed T. Finite element simulations of free convection flow inside a porous inclined cavity filled with micropolar fluid. J Porous Media. 2021;24(2):57-75.
[40] Ali N, Nazeer M, Javed T, Razzaq M. Finite element analysis of bi-viscosity fluid enclosed in a triangular cavity under thermal and magnetic effects. Eur Phys J Plus. 2019;134:2.
[41] Patel ED, Kumar S. Thermal performance of a single loop pulsating heat pipe with asymmetric adiabatic channel. Appl Therm Eng. 2023;219:119541.
[42] Li G, Li J. Thermal characteristics of a flat plate pulsating heat pipe module for onsite cooling of high-power server CPUs. Therm Sci Eng Prog. 2023;37:101542.
[43] Yang Z, Zhang Y, Bai L, Zhang H, Lin G. Experimental study on the thermal performance of an ammonia loop heat pipe using a rectangular evaporator with longitudinal replenishment. Appl Therm Eng. 2022;207:118199.
[44] Xu H, Yang Y, Gan K, Zhang H, Gao Y, Li R, et al. Heat transfer performance of novel high temperature flat heat pipe (HTFHP) with heating power and inclination angles. Appl Therm Eng. 2023;220:119679.
[45] Mirmanto M, Joniarta IW, Sayoga IMA, Nurpatria N, Padang YA, Yudhyadi IGNK. Effect of water volume on a thermoelectric cooler box performance. Front Heat Mass Transf. 2018;11:1-9.
[46] Hashimoto M, Akizuki Y, Sato K, Ueno A, Nagano H. Proposal, transient model, and experimental verification of loop heat pipe as heating device for electric-vehicle batteries. Appl Therm Eng. 2022;211:118432.

[47] Abela C, Mameli M, Nikolayev V, Filippeschi S. Experimental analysis and transient numerical simulation of a large diameter pulsating heat pipe in microgravity conditions. Int J Heat Mass Transf. 2022;187:122532.
[48] Huaqi L, Zeyu O, Xiaoyan T, Li G, Da L, Xiaoya K, et al. The development of high temperature heat-pipe transient model for system analysis of heat pipe cooled microreactor. Prog Nucl Energy. 2022;146:104145.
[49] Ma Y, Tian C, Yu H, Zhong R, Zhang Z, Huang S, et al. Transient heat pipe failure accident analysis of a megawatt heat pipe cooled reactor. Prog Nucl Energy. 2021;140:103904.
[50] Zhang Z, Chai X, Wang C, Sun H, Zhang D, Tian W, et al. Numerical investigation on startup characteristics of high temperature heat pipe for nuclear reactor. Nuclear Engineering and Design. 2021;378:111180.

Appendix

Table A1 Temperature profile results from numerical and laboratory experiments with T_i = 70 °C

Time [s]	Temperature [°C]					
	Numerical results			Laboratory results		
	Evaporator	Adiabatic	Condenser	Evaporator	Adiabatic	Condenser
0	25.0000	25.0000	25.0000	25.0	25.0	25.0
100	34.9038	29.4017	23.8996	30.3	29.1	24.1
200	43.3055	33.1358	22.9661	35.0	29.8	23.0
300	49.5556	35.9136	22.2716	38.6	31.0	22.2
400	54.3343	38.0375	21.7406	41.8	32.7	21.5
500	57.9956	39.6647	21.3338	45.0	34.3	20.9
600	60.8011	40.9116	21.0221	48.1	36.6	20.1
700	62.9510	41.8671	20.7832	51.2	37.9	20.1
800	64.5984	42.5993	20.6002	54.3	38.8	20.1
900	65.8608	43.1604	20.4599	57.4	40.0	20.1
1000	66.8282	43.5903	20.3524	60.4	41.3	20.1
1100	67.7695	43.9198	20.2701	62.6	42.3	20.0
1200	68.5728	44.3657	20.1215	64.4	42.3	20.1
1300	69.4063	44.6275	20.0931	65.8	42.3	20.0
1400	**70.0000**	**45.0000**	**20.0000**	**65.8**	**42.4**	**20.1**
1500	70.0000	45.0000	20.0000	65.8	42.3	20.1
1600	70.0000	45.0000	20.0000	65.7	42.3	20.0
1700	70.0000	45.0000	20.0000	65.7	42.3	20.0
1800	70.0000	45.0000	20.0000	65.6	42.4	20.1

Table A2 Temperature profile results from numerical and laboratory experiments with T_i = 80 °C

Time [s]	Temperature [°C]					
	Numerical results			Laboratory results		
	Evaporator	Adiabatic	Condenser	Evaporator	Adiabatic	Condenser
0	25.0000	25.0000	25.0000	25.0	25.0	25.0
100	37.1047	30.5021	23.8996	32.9	27.8	24.3
200	47.3734	35.1697	22.9661	45.4	30.0	23.3
300	55.0125	38.6420	22.2716	51.6	31.5	22.9
400	60.8530	41.2968	21.7406	55.6	33.2	22.4
500	65.3279	43.3309	21.3338	58.4	37.7	21.8
600	68.7569	44.8895	21.0221	61.1	39.7	21.3
700	71.3845	46.0839	20.7832	62.7	41.3	20.2
800	73.3980	46.9991	20.6002	64.2	41.8	20.0
900	74.9410	47.7005	20.4599	65.6	43.2	19.9
1000	76.1233	48.2379	20.3524	66.7	44.6	20.1
1100	77.0293	48.6497	20.2701	68.0	44.9	19.9
1200	77.7236	48.9653	20.2070	69.9	46.5	20.1
1300	78.2556	49.2071	20.1586	70.9	47.0	20.0
1400	78.6633	49.3924	20.1215	71.9	47.0	20.0
1500	78.9757	49.5344	20.0931	73.0	47.1	20.1
1600	79.3985	49.7905	20.0419	73.6	47.1	20.0
1700	79.7293	49.8770	20.0246	74.5	47.1	20.0
1800	**80.0000**	**50.0000**	**20.0000**	**75.5**	**47.0**	**20.1**
1900	80.0000	50.0000	20.0000	75.5	47.0	20.0
2000	80.0000	50.0000	20.0000	75.5	46.9	20.1
2100	80.0000	50.0000	20.0000	75.5	47.0	20.0
2200	80.0000	50.0000	20.0000	75.5	47.0	19.9
2300	80.0000	50.0000	20.0000	75.5	47.0	20.3

Table A3 Temperature profile results from numerical and laboratory experiments with T_i = 90 ºC

Time [s]	Temperature [ºC]					
	Numerical results			Laboratory results		
	Evaporator	Adiabatic	Condenser	Evaporator	Adiabatic	Condenser
0	25.0000	25.0000	25.0000	25.0	25.0	25.0
100	33.4002	25.9529	24.5091	32.7	26.9	24.3
200	42.3466	28.1742	23.5141	38.9	27.6	23.3
300	50.3440	30.2445	22.6962	44.0	28.5	22.9
400	57.2727	32.7927	22.0664	48.8	29.3	22.4
500	63.0000	35.0734	21.5836	53.7	29.9	21.8
600	68.0000	37.0817	21.2137	58.3	30.8	21.3
700	72.5000	38.8425	20.9302	63.0	31.7	20.2
800	76.0000	40.3845	20.7129	67.5	32.8	20.0
900	78.9000	41.7344	20.5465	71.8	33.9	19.9
1000	81.1000	42.9161	20.4189	74.9	35.0	20.1
1100	82.8000	43.9505	20.3212	77.2	36.8	19.9
1200	83.9000	44.8560	20.2462	78.9	37.5	20.1
1300	84.8000	45.6486	20.1889	80.0	38.8	20.0
1400	85.5000	46.3424	20.1449	81.0	39.4	20.0
1500	86.4000	46.9497	20.1112	82.0	40.0	20.1
1600	87.0000	47.4813	20.0853	83.9	41.1	20.0
1700	87.7000	47.9467	20.0656	84.6	41.9	20.0
1800	88.2000	48.3541	20.0504	85.2	42.0	20.1
1900	88.5000	48.7106	20.0388	86.6	43.2	20.0
2000	89.1000	49.0228	20.0299	88.4	43.7	20.1
2100	89.6000	49.2960	20.0167	88.0	43.9	20.0
2200	**90.0000**	**49.5352**	**20.0044**	**88.3**	**44.0**	**19.9**
2300	90.0000	50.0000	20.0000	88.4	44.0	20.1
2400	90.0000	50.0000	20.0000	88.5	44.0	20.1
2500	90.0000	50.0000	20.0000	88.6	44.0	20.1